Received: 22 December 2020 | Revised: 2 April 2021 | Accepted: 2 April 2021

DOI: 10.1002/app.50879

ARTICLE

Applied Polymer SCIENCE WILEY

Upgrading poly(styrene-co-divinylbenzene) beads: Incorporation of organomodified metal-free semiconductor graphitic carbon nitride through suspension photopolymerization to generate photoactive resins

Cansu Esen | **Markus Antonietti** | **Baris Kumru**

Department of Colloid Chemistry, Max Planck Institute of Colloids and Interfaces, Potsdam, Germany

Correspondence
Baris Kumru, Department of Colloid Chemistry, Max Planck Institute of Colloids and Interfaces, Am Mühlenberg 1, 14476 Potsdam, Germany.
Email: baris.kumru@mpikg.mpg.de

Funding information
Max Planck Society

Abstract

The inclusion of the metal free semiconductor graphitic carbon nitride (g-CN) into polymer systems brings a variety of new options, for instance as a heterogeneous photoredox polymer initiator. In this context, we present here the decoration of the inner surface of poly(styrene-co-divinylbenzene) beads with organomodified g-CN via one pot suspension photopolymerization. The resulting beads are varied by changing reaction parameters, such as, crosslinking ratio, presence of porogens, and mechanical agitation. The photocatalytic activity of so-formed beads was tested by aqueous rhodamine B dye photodegradation experiments. Additionally, dye adsorption/desorption properties were examined in aqueous as well as in organic solvents. Photoinduced surface modification with vinylsulfonic acid and 4-vinyl pyridine is introduced. Overall, metal-free semiconductor g-CN donates photoactivity to polymer networks that can be employed for dye photodegradation and acid–base catalyst transformation through facile photoinduced surface modifications.

KEYWORDS

catalysts, crosslinking, photochemistry, photopolymerization, porous materials

1 | INTRODUCTION

Semiconductors for photochemical purposes, for example, for energy harvesting, water treatment and pollution degradation, usually suffer from sustainability and toxicity issues, taking lead or cadmium derivatives as an example. Considering this, graphitic carbon nitride (g-CN) as a metal-free semiconductor is an alternative to be investigated, bringing advantages such as ease of handling, low cost, and low toxicity as well as showing a sufficient photocatalytic activity under visible light.[1–6] As a heterogeneous photocatalyst, it has been used in many applications such as water splitting, hydrogen evolution, CO_2 reduction and degradation of aqueous contaminants.[3,7–10] Moreover, tunable morphology and composition along with the facile functionalization brings a rich chemical diversity.[11–13] Very recent review by Zhang and colleagues nicely describes the synthesis of diverse carbon nitride materials and their corresponding electronic properties and applications, thus underlining the emergent interest on g-CN family.[14] For instance, tailored g-CN nanosheets from 2D layers to 3D network by

reversible assembly resulted in a functional hydrogel network exhibiting high selectivity for dye extraction.[15] g-CN was also described as a radical photoinitiator for radical polymerization reactions by a photoredox initiation mechanism.[16–18] Hydrogels made as such proved that the (left-in) carbon nitride not only acted as a photoinitiator, but also mechanically reinforced the resulting hybrid gels.[19] In emulsion polymerization, g-CN could act as a photoinitiator and a Pickering stabilizer.[20] Lately, g-CN was employed in an inverse suspension photopolymerization as a water dispersible photoinitiator to obtain recollectable macrohydrogel beads with the purpose of wastewater treatment under visible light.[21] When the dispersibiliy of g-CN was altered in a solid-state matrix, high-performance PL sensor was fabricated in a cost and time efficient way.[22] In organic media, the poor organic dispersibility of g-CN (which is due to the strong aggregation of the 2d-sheets by stacking interactions) was the main challenge to overcome. This problem could be efficiently solved by functionalizing phenyl-doped g-CN with vinyl-thiazole under visible light irradiation. The as-made vinyl thiazole grafted g-CN (vTA-CMp) demonstrated excellent organodispersibility based on organo-electrostatic stabilization via edge-induced surface modification.[23] Since then, surface modified vTA-CMp has been applied in organic media.[24,25]

For the present subject of making porous polymer beads as supports for adsorption and catalysis, suspension polymerization is the industrial method of choice. In a typical suspension polymerization; the organic phase (initiator, monomer, and solvent/nonsolvent as porogen) is dispersed in aqueous media with a stabilizer, and proper shear or mechanical agitation is applied in order to result in uniform, stable droplets which are then later converted into the corresponding polymer beads. Reaction conditions include physical parameters, such as stirring speed, temperature, time, or equipment dimensions, and chemical parameters as monomer, initiator, cross-linker and diluent can be altered.[26] Standard recipes operated on industrial scale include styrene mixed with different cross-linkers such as divinylbenzene (DVB), ethylene glycol dimethylacrylate (EGDMA) and triethylene glycol dimethylacrylate (TEGMA),[27,28] resulting for instance in polystyrene–divinylbenzene (PS-co-DVB) resins. Since its first availability as a sulfonated PS-co-DVB resin by D'Alelio in 1944,[29] its high potential as a heterogeneous catalyst has been explored, and possible advantages over homogeneous acid catalysts, that is, recyclability, clean-processes, matrix selectivity, by-product elimination and long-term storage, were described.[30–33] Over the years, numerous structural variations from microreticular to macroporous and hyperbranched structures were accomplished, and all served well in many different applications,[34,35] such as, water treatment,[36–41] catalyst support,[42–45] immobilization of enzymes,[46] and templates for nanoparticle growth.[47,48] Novel functionalities that would extend the viability of PS-co-DVB are still strived.

Furthermore, the covalent modification of chemically inactive PS-DVB beads[49] is problematic which hinders the integration of further surface functionalities. Common functionalities involve a cross-linked bead copolymer modified by sulfonation,[50,51] chloromethylation,[52] and amination.[53,54] Other derivatization techniques include Friedel-Crafts alkylation and acylation and introduction of complex ligands.[55] Indeed, most of these techniques require corrosive and toxic chemicals, which limits the feasibility and sustainability of final production, that is, to PS-DVB matrix is boiled by mixture of acetic anhydride and concentrated sulfuric acid to attain sulfonation.[56] Another method to access surface modification requires the addition of a third monomer, such as 4-chloro styrene and vinyl methl ketone, both that are more prone to modification compared to PS and DVB, or an addition of a monomer which possesses an acidic or basic functionality.[57,58] This is why we intended to develop a remarkably simplified and more sustainable synthesis process, based on hybrids with carbon nitride.

For that, organodispersible vTA-CMp nanosheets will be added to the oil phase composed of styrene, divinylbenzene, and an organic porogen, and further photopolymerization will be performed to integrate the carbon nitride nanosheets into the polymer structure located at the interface as a cross-linking, multifunctional initiator (Scheme 1). The stability of the recipe will be examined by varying the amount of cross-linker and and bead sizes, and corresponding characterizations will be enclosed. Furthermore, photoactivity of the final beads will be confirmed by aqueous RhB photodegradation and organic character of the beads will be addressed via organic dye adsorption experiments. A brief insights into the possibility of a photo-induced surface modification will be exhibited.

2 | EXPERIMENTAL SECTION

Materials: 1-octanol (≥99%, Sigma Aldrich), 4-vinylpyridine (VP, 95%, 100 ppm hydroquinone as inhibitor, Sigma-Aldrich), 2,4-diamino-6-phenyl-1,3,5 triazine (Mp, 97%, Sigma-Aldrich), 2,2′-Azobis(2-methylpropionitril) (AIBN, % 98 Sigma-Aldrich), 2,4,6-Trimethylbenzoyl diphenylphosphine oxide (DPO, 98%, Sigma-Aldrich), 4-methyl-5-vinylthiazole (vTA, 97%, Sigma-Aldrich), basic aluminum oxide, cyanuric acid (C, 98%, Sigma-Aldrich), divinylbenzene (DVB, ≥99%, 4-tert-butylcatechol as stabilizer, Sigma-Aldrich), hydrochloric acid (HCl, 37%, Sigma-Aldrich), *N,N*-Dimethylformamide (DMF, ≥99, Sigma-Aldrich), perylene (Sigma-Aldrich), polyvinyl alcohol (PVA, fully hydrolyzed,

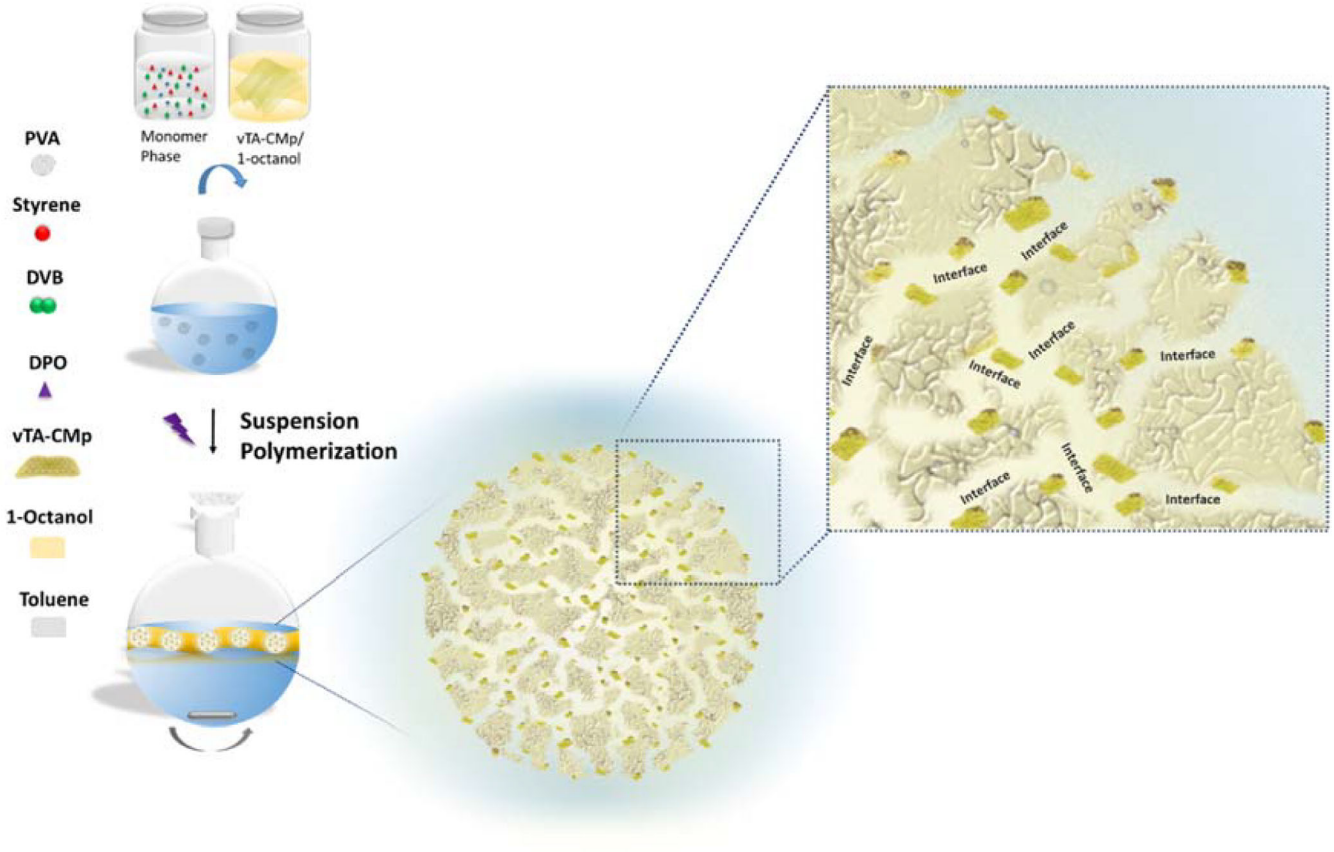

SCHEME 1 Schematic overview of organomodified g-CN (vTA-CMp) incorporation into PS-DVB beads via suspension photopolymerization [Color figure can be viewed at wileyonlinelibrary.com]

approx. 145,000 Da), rhodamine B (RhB, 95%, Sigma-Aldrich), sudan red 7B (Sigma-Aldrich), styrene (St, ≥99%, 4-tert-butylcatechol as stabilizer, Sigma-Aldrich), tetrahydrofuran (THF, anhydrous 99.9%, HPLC grade, Sigma-Aldrich), toluene (anhydrous 99.8%, Sigma-Aldrich), vinylsulfonic acid sodium salt solution (VSA, 25 wt% in water, Sigma-Aldrich). St and DVB were passed through basic alumina column prior to use to remove the inhibitor. Phenyl doped g-CN (CMp) synthesis and its corresponding vinyl thiazole modification (vTA-CMp) were conducted according to the cited literature.[23] Ultraviolet (UV) light irradiation was performed via 30 W UV chip (Fdit 395-400 Nm UV LED) connected to a self-made circuit and a cooling system. Visible light irradiation was implemented via two 50 W LEDs (Chip Bulb Light DIY White 3800LM 6500 K) connected to a self-made circuit and a cooling system.

Characterization: X-ray diffraction (XRD) patterns of reference, BT5m and CBT5m beads grinded via ball mill were obtained by using a Bruker D8 Advance X-ray diffractometer via Cu Kα radiation. Scanning electron microscopy (SEM) was performed using a JSM-7500F (JEOL) microscope equipped with an Oxford Instruments X-Max 80 mm^2 detector for the determination of both elemental composition and morphology for reference and model beads. Fourier transform infrared (FTIR) spectra were acquired on a Nicolet iS 5 FTIR spectrometer. Solid-state ultraviolet–visible (UV–vis) spectroscopy was performed via a Cary 500 Scan spectrophotometer equipped with an integrating sphere. Thermogravimetric analysis (TGA) was performed via TG 209 Libra from Netzsch in nitrogen atmosphere with heating rate 10 K min^{-1} using aluminum crucible for samples. Photoluminescence spectra (PL) of the reference, BT5m, CBT5m powdered beads were obtained by a Hitachi F-7000 spectrometer. Fluorescence images of reference and BT5m were obtained by confocal laser scanning microscopy (CLSM, TCS SP5, Leica, Germany). vTA-CMp/1-octanol suspension was prepared in a sonication bath at 50% amplitude from Elma (Transsonic T310). Optical microscopy images were taken by Olympus BX41. Combustive elemental analysis of CBT5m-VSA and CBT5m-VP were recorded via a Vario Micro device.

Solvent uptakes of the beads were calculated manually. 20 mg (*Wd*) dried beads were put into two separate vials, one with 1 ml water and the other with 1 ml toluene, then capped and left for 24 h at room temperature.

Beads treated with solvent were weighted separately (*Ws*), and solvent uptake was calculated by using the following formula for each solvent type and bead:

$$Solvent\ uptake = \frac{Ws - Wd}{Wd} \times 100\% \quad (1)$$

Synthesis of phenyl doped g-CN (CMp):Phenyl-modified g-CN (CMp) was synthesized according to literature.[59] 1.3 g of cyanuric acid and 1.8 g of 2,4-diamino-6-phenyl-1,3,5-triazine were weighed and mixed with 50 ml distilled water and shaken overnight. After centrifugation at 5000 rpm for 5 min, the precipitate was dried at 60°C under vacuum overnight. The dried product is transferred into a capped crucible and put into N_2 protected oven at 450°C for 2 h, with a heating rate of 2.3°C/min. After cooling to ambient temperature, yellow CMp powder was obtained and well grinded prior to use.

Synthesis of organodispersible vTA-CMp via vinyl thiazole photografting: vTA-CMp particles were synthesized according to the cited literature.[23] 100 mg CMp was mixed with 1 ml vTA and sonicated for 5 min in a sonic bath. Mixture was degassed with nitrogen flux for 10 min and placed between 2 50 W LEDs and stirred for 3 h under continuous visible light irradiation and for purification, the mixture was filtered and washed with ethanol 3 times (20 ml each portion) and dried under vacuum at 60°C overnight. After cooling to ambient temperature, dark-yellow vTA-CMp powder was obtained and well grinded before usage.

Preparation of vTA-CMp /1-octanol suspension: In order to obtain well dispersed vTA-CMp /1-octanol dispersion, the bulk vTA-CMp was sonicated to exfoliate carbon nitride. 100 mg vTA-CMp and 8 ml of 1-octanol were added to a 10 ml plastic centrifuge tube then exfoliated in a sonic bath for 3 times/30 min cycles. The dispersion was set to rest for 1 h prior to use in order to allow a sedimentation of larger particles.

Synthesis of beads via suspension photopolymerization: Various PS-DVB-vTA-CMp beads were termed according to indicated parameters: Crosslinking ratio (numbering), solvent presence (T), agitation speed (m-medium 700 rpm, s-slow 400 rpm), vTA-CMp as photoinitiator (C). For example; a Model bead, BT5m, was prepared by DPO as photoinitiator, 25% DVB to Styrene, a defined amount of toluene added, stirred at a medium speed. A second example: CBT5m beads were prepared in the same way with BT5m except for DPO photoinitiator addition, herein vTA-CMp nanosheets were utilized as a photoinitiator.

The reference beads (PS-DVB) are the same as with BT5m and only differ by the presence of vTA-CMp.

General procedure using BT5m as an example 0.025 g photo-initiator weighed in a glass vial, dissolved in 0.5 ml toluene, followed by the addition of 1.1 ml styrene, 0.55 ml DVB, and 0.5 ml vTA-CMp dispersion (monomer phase). On the other side, 15 ml PVA/water solution (1 wt%) was prepared in 25 ml round bottom flask. Afterwards, the organic phase was injected into the flask. The flask was capped with a glass cap, placed in front of an Ultraviolet source (10 cm apart from flask) at 700 rpm on a magnetic stirrer for 8 h to complete a photoinduced suspension polymerization. After 4 h, liquid monomer droplets began to solidify distinctively. After 8 h, the solidified beads were filtered and transferred into a glass petri dish, where solvent evaporation at ambient temperature was performed over 2 days in the fume hood in order to avoid any possible cracking via temperature-induced drying. Then after, solid and dried PS-DVB-vTA-CMp were ready for further use.

Bead synthesis by thermal initiator: 0.025 g thermal initiator (AIBN) weighed in a glass vial, dissolved in 0.2 ml toluene, followed by the addition of 1.1 ml styrene, 0.35 ml DVB and 0.5 ml 1-octanol. 15 ml water phase consisting 1 wt% PVA was poured in 25 ml round bottom flask and purged with nitrogen for 15 min. After purging, organic phase was injected into the flask and the mixture was purged with nitrogen for another 15 min, then the flask was capped with a glass cap and placed in an oil-bath under stirring at 700 rpm with a magnetic stirrer. The temperature was gradually increased from room temperature to 60°C in 1 h and left at 60°C for 1 h to initiate the polymerization. After 2 h in total, temperature was gradually increased again every 15 min until reaching 70°C in 1 h and left for 1 h at 70°C. After 4 h, solidified beads were filtered, washed 2 times with THF and dried in a vacuum oven overnight, labeled as Reference bead (I-Ref). Alternatively, 0.025 g thermal initiator (AIBN) weighed in a glass vial, dissolved in 0.2 ml toluene, followed by the addition of 1.1 ml styrene, 0.35 ml DVB and 0.5 ml vTA-CMp 1-octanol dispersion. 15 ml water phase consisting 1 wt% PVA was poured in 25 ml round bottom flask and purged with nitrogen for 15 min. After purging, organic phase was injected into the flask and the mixture was purged with nitrogen for another 15 min, then the flask was capped with a glass cap and placed in an oil-bath under stirring at 700 rpm with a magnetic stirrer. The temperature was gradually increased from room temperature to 60°C in 1 h and left at 60°C for 1 h to initiate the polymerization. After 2 h in total, temperature was gradually increased again every 15 min until reaching 70°C in 1 h and left for 1 h at 70°C. After 4 h, solidified beads were filtered, washed 2 times with THF and dried in a vacuum oven overnight, labeled as Model bead (I-Model).

Surface Photomodification of PSDVB-vTA-CMp Beads via VSA and VP: Photo-induced surface

modification via VSA was performed by following this procedure: 0.050 g CBT5m beads were weighted in a glass vial and 3 ml VSA:DMF (2:1 vol%) mixture was injected, thereafter vial was capped and left for 30 min to complete adsorption–desorption equilibrium under medium magnetic stirring. Afterwards, visible light irradiation was performed via white 50 W LED (Chip Bulb Light DIY White 3800LM 6500 K) overnight (∼12 h). Beads were filtered and washed with 10 ml deionized water:DMF (1:1 v%) 3 times and left overnight in water:DMF (2:1 vol.%) mixture. After purification, they were dried in a vacuum oven overnight.

Photo-induced surface modification via VP was performed by following this procedure: 0.050 g CBT5m beads were weighted in a glass vial and 3 ml VP was injected thereafter vial was capped and left for 30 min to complete adsorption–desorption equilibrium under medium magnetic stirring. Afterwards, visible light irradiation was performed via white 50 W LED (Chip Bulb Light DIY White 3800LM 6500 K) overnight (∼12 h). Beads were filtered and washed with 10 ml ethanol 3 times and left overnight in toluene. After purification, they were dried in a vacuum oven overnight.

Photocatalytic RhB degradation: The photocatalytic activity of PS-DVB-vTA-CMp beads were investigated via photocatalytic degradation of aqueous RhB solution (2 ppm in deionized water) under visible light irradiation. As an example procedure of RhB degradation experiment, for each sample: 55 mg beads and 1.5 ml RhB dye solution were mixed in a glass vial in the dark under continuous stirring for 30 min in order to complete an adsorption–desorption equilibrium. Afterwards, the irradiation was performed by a white 50 W LED (Chip Bulb Light DIY White 3800LM 6500 K) under continuous stirring for 5 h. Additionally, the same procedure was applied additionally without visible light irradiation to all samples.

A recycled photocatalytic activity test was carried out by following the above-mentioned process. A certain amount of RhB solution in suspension was withdrawn every 1 h and RhB absorption was followed by spectrophotometrically. After completing each cycle, employed beads were collected, washed by immersing in deionized water, and dried overnight. Additionally, the same procedure only with one run cycle was applied without visible light irradiation to BT5m and CBT5m samples (dark measurements).

The kinetic experiment of pristine vTA-CMp for RhB degradation was assessed by the following procedure; vTA-CMp/RhB solution (1 $g.L^{-1}$) was prepared and after 30 min of adsorption/desorption equilibrium, set in front of a visible light source. Every 30 min, 1 ml sample was collected from suspension, centrifuged for 5 min at 10000 rpm then investigated via UV–visible spectroscopy to follow RhB degradation.

pH effect on photodegradation of RhB was investigated by conducting RhB stock solution adjusted with 1 M HCL and 1 M NaOH solutions to pH 2, pH 7, and pH 13 values and one run cycle kinetic measurement procedure (1 h time interval) was applied as described.

Aqueous RhB dye adsorption & desorption: Model (BT5m) and reference beads were weighted in two glass vials containing aqueous RhB solution (0.055 g beads/1.5 ml), then the vials were capped and left in the dark for 24 h in order to investigate the adsorption performance. After 24 h, RhB dye adsorbed model and reference beads were separately immersed into glass vials containing 1 ml deionized water and left in the dark for an additional 24 h for the desorption. Afterwards, the desorption performance was measured the same way as adsorption measurement. Adsorption/desorption recycle test was evaluated according to the described procedure. To investigate pH effect on adsorption/desorption activity, above-mentioned procedure was performed by conducting as-prepared RhB solutions at pH 2, pH 7, and pH 13 to model bead and every 24-h certain amount of RhB solution was withdrawn from suspension to monitor RhB absorption at λ_{max} (554 nm) via UV–vis spectroscopy.

Oil-soluble dye adsorption in biphasic system & desorption: Model (BT5m) beads were weighted separately in two glass vials containing deionized water (0.050 g beads/4 ml) and shaken for 20 s. Following that, 50 µl Sudan Red 7B and perylene solutions (200 ppm in toluene) were separately injected into the vials and adsorption performance was investigated by taking digital photos in every 5 min for 30 min. Thereafter, dye soaked beads were immersed into 4 ml toluene and dye releasing performance was followed by taking digital photos after 1 and 3 h. Following that, as a second releasing round, partially dye desorbed beads were immersed in 4 ml toluene and dye releasing performances were monitored by taking digital photos after 10 min, 1 and 24 h.

3 | RESULTS AND DISCUSSION

3.1 | Bead synthesis

The organic phase consisting of St, DVB, toluene and a photoinitiator was prepared by varying conditions and ratios as indicated in Table 1. Considering suspension polymerization, controlling bead size by agitation speed is a standard practice. Moreover, as the amount of crosslinker is affecting both surface morphology and porosity, its amount was varied 25, 35, and 50 wt%. Furthermore,

TABLE 1 Preparation parameters of PS-co-DVB beads with vTA-CMp

	Crosslinker (DVB %)[a]			Solvent (toluene)		Photoinitiator		Stirring rate (rpm)	
Beads	**25**	**35**	**50**	**Incl.**	**Excl.**	**DPO**	**VTA-CMp**	**400**	**700**
BT5m	x			x		x			x
BT7m		x		x		x			x
BT10m			x	x		x			x
B5m	x				x	x			x
BT5s	x			x		x		x	
CBT5m	x						x		x
REF[b]	x			x		x			x

[a]DVB ratios are in relation to Styrene.
[b]Reference beads were prepared without vTA-CMp.

presence and absence of solvent during polymerization is also investigated in order to examine its role onto final bead size.

Meanwhile, the vTA-CMp/1-octanol dispersion is prepared in another vial, then together with monomer phase they are injected in 25 ml round bottom flask containing 15 ml PVA/water (1 wt%) solution. The flask is capped, and polymerization is initiated via UV light. Efficient reaction time is determined to be 8 h along with the constant adequate agitation for all beads except for CBT5m, which is the one with vTA-CMp as photoinitiator and requires 10 h under UV light irradiation.

In order to investigate the integration of vTA-CMp, the resulting BT5m, CBT5m, and reference beads were characterized via XRD (Figure 1(a)). Diffraction between 17° and 20° can be attributed to the layer-layer stacking of aromatics and patterns show similar profile arising from PS-DVB nature. The peak located at 27.6° that is observed for carbon nitride containing samples BT5m and CBT5m can be assigned to carbon nitride 002 plane diffraction. Following that, FTIR spectra (Figure 1(b)) were also examined as well. Firstly, as a general peak assignment regarding the copolymer formation, from 3106 to 3030 cm^{-1} indicates C—H aromatic stretching, from 2365 to 2330 cm^{-1} shows aromatic overtones, the region in between 1600 and 1400 cm^{-1} corresponds to C—C aromatic stretching, at fingerprint region from 1080 to 985 in-plane C—H bending and lower fingerprint region shows out-of-plane C—H bending. All spectra display similar characteristic peaks that might be associated with low amount of vTA-CMp into the beads (around 4 wt%).

Moreover, solid UV–Vis spectra comparison between reference bead, model bead and vTA-CMp powder shows the specific broadening of BT5m from 209 to 334 nm, which is significantly different than a reference bead spectrum (no photoactivity is expected from the reference bead) and can be assigned to the presence of vTA-CMp as it matches with the pure vTA-CMp spectrum (Figure 1(c)). Furthermore, TGA measurement (Figure 1(d)) demonstrated that the vTA-CMp incorporation enhances thermal resistance of the beads (on 85% weight loss point, reference bead at 378°C and model bead at 404°C) therefore vTA-CMp acts a filler as well. Moreover, photoluminescence spectroscopy was employed in order to gain more insight into optical properties of synthesized beads (Figure 1(e)). Considering the previous work of our group, 380 nm excitation wavelength was reported as optimum for PL study, so the same excitation wavelength was chosen to investigate polymer beads. As expected, almost no signal was received from reference bead, and strong spectra were recorded for vTA-CMp containing beads that possess a similar profile to pure vTA-CMp.[23] An interesting phenomenon is observed when vTA-CMp is employed as a photoinitiator, meaning that when it has covalent interaction with the polymer network, then the intensity of the spectra decreases compared to its embedded analogue. This leads to a conclusion that contrary to a common belief, an insulator aromatic polymer has an influence on the photodynamics of an excited semiconductor (partial hole transfer) once attached covalently, which was observed very recently in PS grafted g-CN thin films as well.[60]

In order to examine the morphology of the model (BT5m), scanning electron microscopy is performed and shown in combination with the optical microscope images in Figure 2. All images exhibit the acquired pore structure and surface roughness based upon formed holes and cavities leading to visually observable internal and external porosity for model bead (Figure 2(a)). The presence of 1-octanol played a significant role in producing relatively porous PS-DVB-vTA-CMp beads via both enabling an integration of vTA-CMp into the organic media and acting as a porogen by exhibiting a template

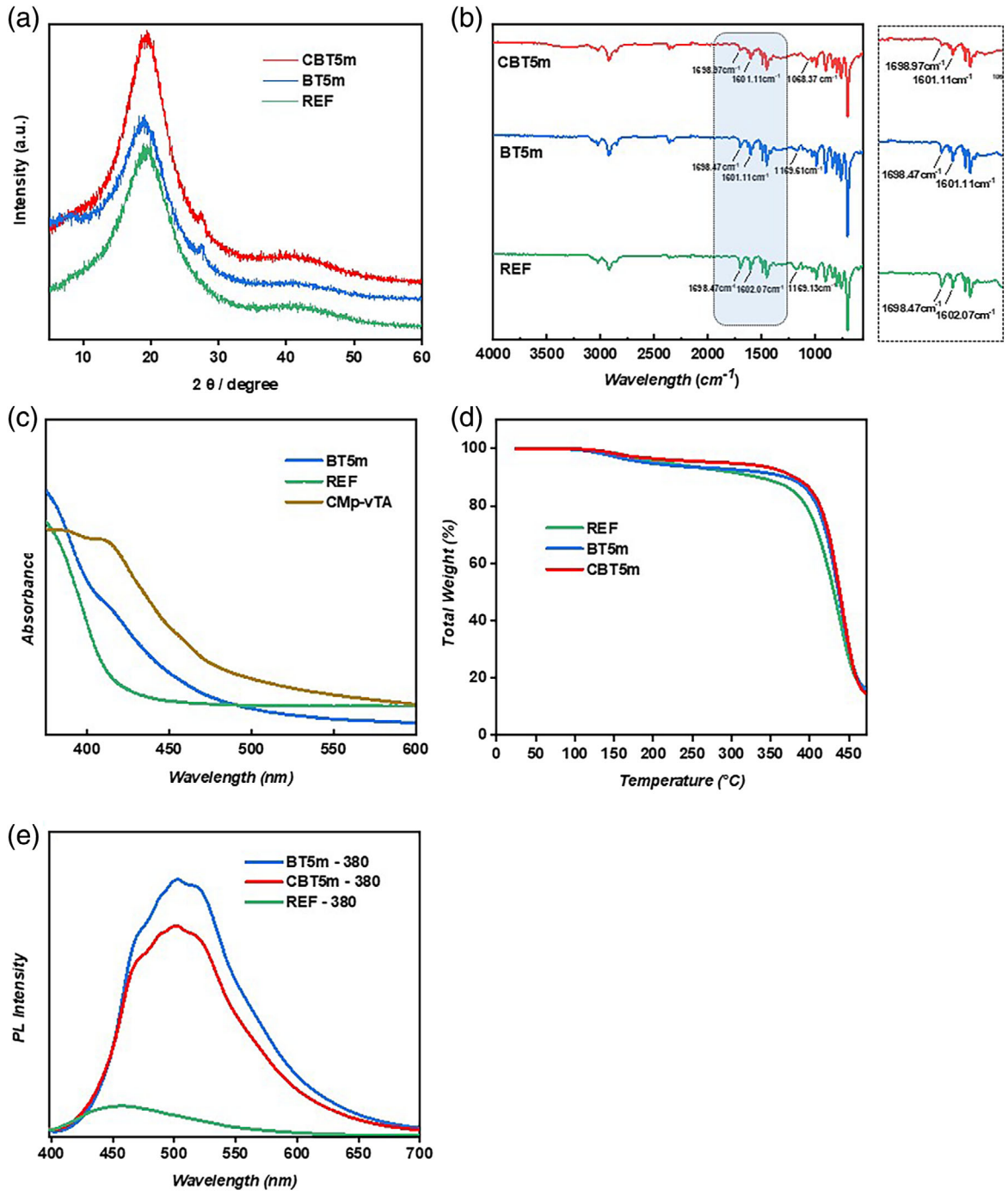

FIGURE 1 (a) XRD profiles and (b) FTIR spectra of the CBT5m, BT5m (model), and reference beads. (c) Solid UV–Vis spectra of BT5m (model), reference beads and pure vTA-CMp powder. (d) TGA measurement of the CBT5m, BT5m (model), and reference beads. (e) Photoluminescence spectra of CBT5m, BT5m, and reference beads at 380 nm excitation wavelength [Color figure can be viewed at wileyonlinelibrary.com]

effect to the network. In addition, we have not attempted to increase the vTA-CMp content in an organic phase at this stage. It is highly important to note that the reaction with non-modified g-CNs does not take place as g-CN does not remain in organic phase in a heterophase system. Despite the commercial porogens in an industry are long chain alkanes such as dodecane, it can not be integrated into vTA-CMp system as it prevents dispersibility, however 1-octanol works successfully in our system.

The reference bead is not expected to bear any nitrogen groups (neither from monomers-photoinitator nor solvent), while the model sample exhibits homogenously

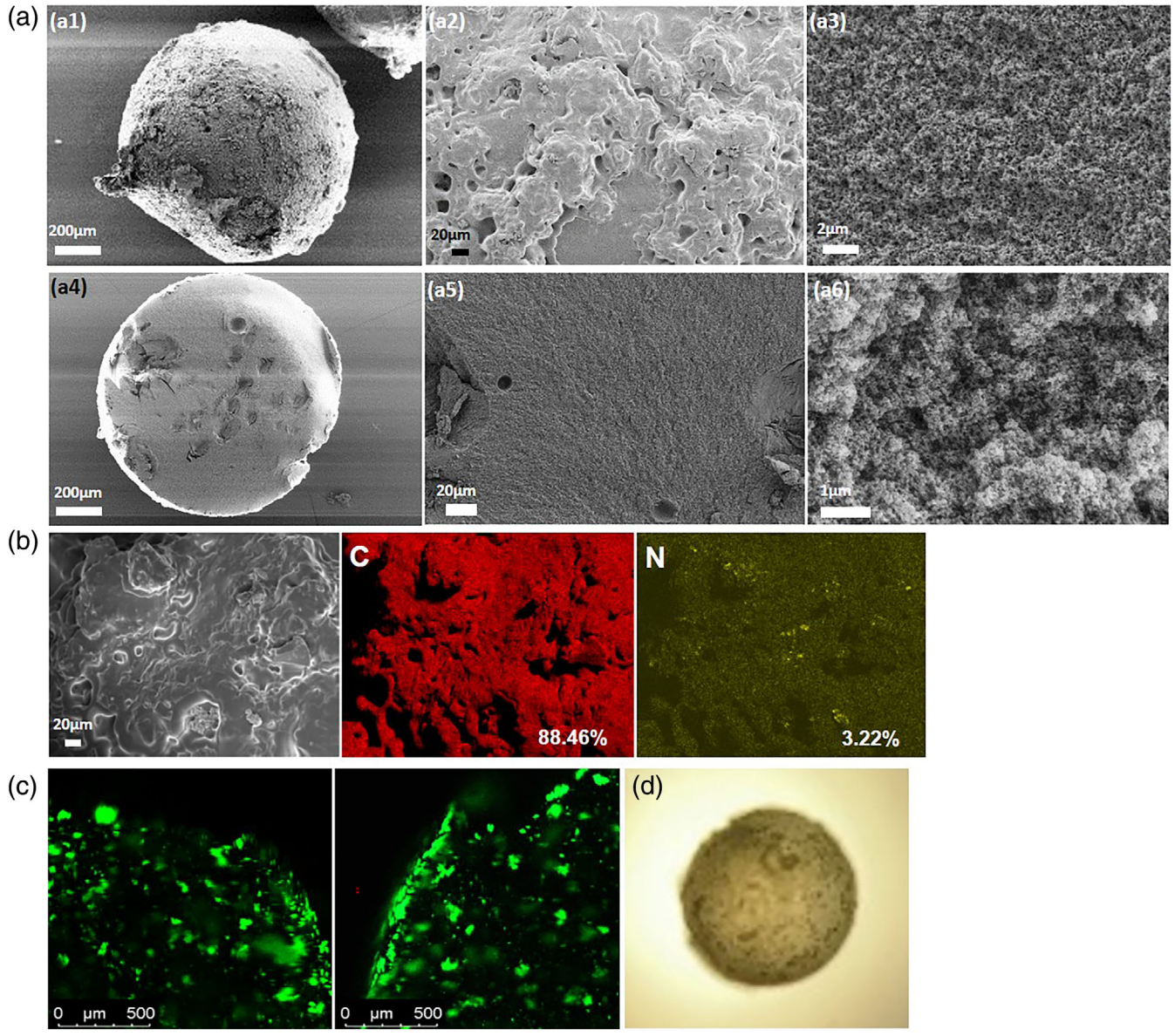

FIGURE 2 Scanning electron microscopy images of (a1-a3) model bead and (a4-a6) its cross-section. (b) Elemental mapping of model bead via EDX, (c) confocal laser scanning microscopy images of toluene immersed model bead from the right and left side, (d) optical microscope image of model bead taken after immersing in toluene [Color figure can be viewed at wileyonlinelibrary.com]

distributed nitrogen atoms as indicated via elemental mapping (with a mass of 3.2% on the investigated area) which highlights the presence of vTA-CMp particles (Figure 2(b)). Based on the homogeneous distribution of nitrogen atoms over the investigated area, one can conclude that the vTA-CMp is fairly distributed in the polymer network. In addition, a major carbon content was monitored as well (with a 88.4% on the investigated area). Another distinct advantage of vTA-CMp that can be useful for applications (here as characterization) is its emissive property (Figure S1). As expected, confocal laser scanning microscopy images clearly present emissive sections on the bead via an intense green luminescence around 540 nm, which arises from vTA-CMp, once again indicating a successful incorporation and a fair distribution (Figure 2(c)).

It is well known that a stabilizer is to be added to the continuous phase to perform a successful suspension polymerization. PVA is one of the most established stabilizer in aqueous phase, which allows a distinct separation of organic spheres and leading to a bead formation of organic phase upon agitation. It is important to underline that our attempts with 31 kDa PVA did not result in well-defined bead formation, while 145 kDa PVA was the

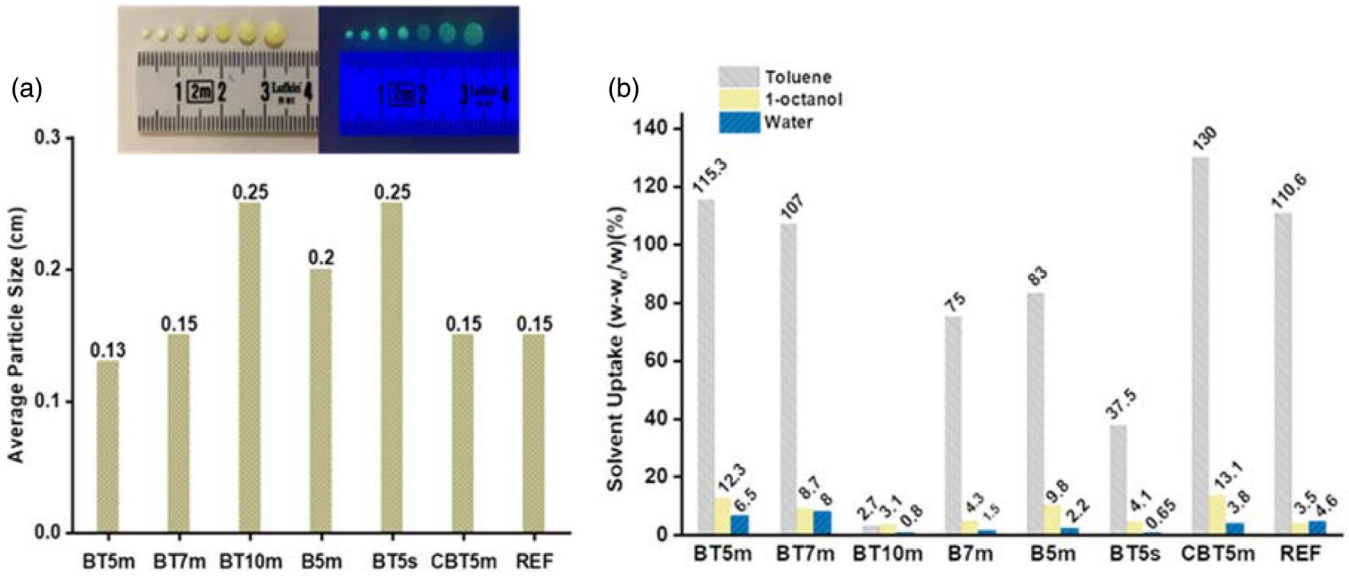

FIGURE 3 (a) Average bead size of PS-co-DVB derived beads along with the size range (measured manually) and corresponding digital images of the tunable bead sizes, (b) solvent uptake ratio measurements performed by 0.020 g beads in 1 ml solvent for 24 h [Color figure can be viewed at wileyonlinelibrary.com]

optimum for the presented reaction systems. In order to take a step closer to industrial processes, we have attempted suspension polymerization by thermal initiator, namely AIBN. For this purpose, a reference bead and a model bead including vTA-CMp-1-octanol dispersion were synthesized. As a result, successful incorporation of vTA-CMp was confirmed via elemental mapping result exhibiting homogenously distributed nitrogen atoms for Model-I bead (Figure S2). Furthermore, based on SEM images, 1-octanol was able to generate porous structures by acting as an anti-solvent in a suspension media during polymerization for both cases (Figure S3), which is a very vital factor as 1-octanol is required to address vTA-CMp in organic phase. The major unconformity which was confronted in terms of reaction parameters was that the miscibility of 1-octanol in water enhances at 70°C which can disrupt the stability of pre-formed suspension droplets leading to undesired clustering, at least in a flask in a lab scale. We have attempted to overcome this problem by temperature settings, and it worths mentioning that the industrial scale integration of vTA-CMp into PS-co-DVB by the help of chemical engineering and parameter-tuning would be highly promising in near future.

The solvent uptake properties of all beads were characterized by immersing the dry beads in water, toluene and 1-octanol over 24 h, and their solvent uptake or water uptake results for all media were calculated by using a mass difference of dry and swollen forms (Figure 3). It is a general knowledge that higher crosslinking leads to a tighter network formation thus less solvent uptake behavior, which was observed in our case studies as well. Considering agitation effect upon solvent uptake property, lowered stirring speed leads to a bigger particle size and resulted in lower solvent uptake performance compared to a sample synthesized via medium stirring speed.

CBT5m interestingly has a slightly higher solvent uptake result than a model bead, this can be correlated synergetic effect since CBT5m is photoinitiated via vTA-CMp, thus a sheet-like vTA-CMp provides a polymerization loci.[20] Water uptake ratios are explicitly lower in comparison with toluene uptake ratios. As expected, based on the organic nature of PS-co-DVB network, there is almost no tendency for water uptake. As a conclusion, most of the vTA-CMp incorporated beads have exhibited significant solvent uptake behavior in toluene.

3.2 | Photocatalytic properties

vTA-CMp incorporation has a distinct advantage regarding photoactivity and such property will be harnessed in the current section (Scheme 2). We have chosen aqueous Rhodamine B (RhB) photodegradation as a model example, which would restrict the photoactivity of the beads solely on the surface as the beads have almost no (to minor) tendency for water uptake.

In terms of reaction condition parameter, the first focus can be put on the model bead analogues (Figure S4a). For the same series, smaller particle size (agitation effect) exhibits an enhanced RhB dye photodegredation activity under visible light irradiation.

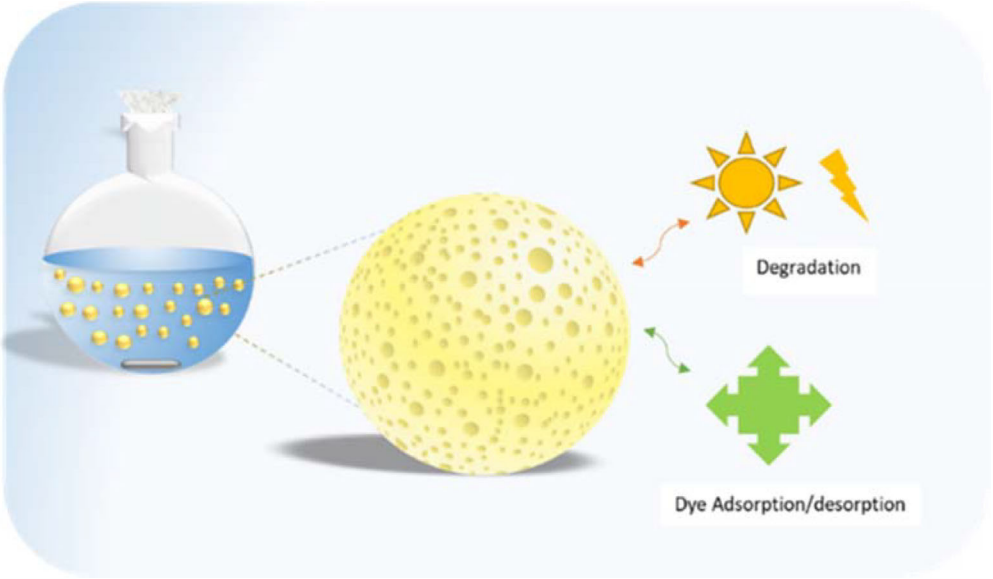

SCHEME 2 The application spectra of vTA-CMp incorporated PS-co-DVB beads. Herein, photocatalytic dye degradation performances of PS-DVB derived beads were recorded via UV–vis spectroscopy. Pure RhB dye solution is included in every experiments as a reference. All prepared samples are irradiated via visible light illumination for 5 h and resulting conclusions were made accordingly (Figure 4) [Color figure can be viewed at wileyonlinelibrary.com]

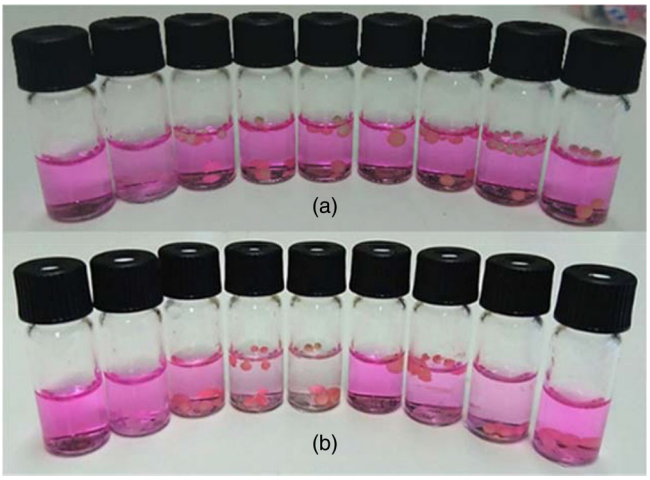

FIGURE 4 Digital images of PS-co-DVB derived beads in RhB solution, from left to right: RhB dye, REF, B5m, BT5m, CBT5m, BT5s, B7m, BT7m, BT10m (a) before visible light irradiation, (b) after 5 h visible light irradiation [Color figure can be viewed at wileyonlinelibrary.com]

During the visible light illumination, absorption of photons by the photocatalyst containing beads leads to a electron–hole pair formation. Subsequently, photogenerated electrons and holes are linked to the formation of active radical species ($HO\cdot$, $O_2^{-\cdot}$, $HO_2^{\cdot}$), which in turn degrade RhB dye molecules in aqueous solution.[21,61–64] Considering the experimental results and degradation mechanism, photodegradation activity can be influenced by the characteristic bead properties such as particle size and porous structure since these vital properties are influencing the interaction between dye molecules and catalytically active surface sites. It has also been noticed that CBT5m, which was initiated via vTA-CMp instead of DPO, has performed highest photodegradation activity toward RhB dye. This result is also in a deal with the PL spectra results of CBT5m, BT5m, and reference beads, which hint towards a possible interaction of vTA-CMp with covalently bound aromatic polymer upon illumination. Following that, increasing crosslinker ratio has decreased the photodegradation activity (Figure S4b), as well as beads synthesized in the absence of toluene (B5m) showed lower photoactivity than the beads synthesized with toluene (BT5m, Figure S4c). The effect of particle size by the means of agitation speed exhibited that the smaller particle size indeed serves an enhanced photoactivity due to more exposed surface (Figure S4d).

Simultaneously, a second sample series including reference bead, BT5m, and CBT5m were left under the dark with the aim of clarifying a potential physical dye adsorption during photodegradation interval (5 h), which can cause a dubious situation over dye degradation by decreasing RhB concentration in water. Apparently, the physical dye adsorption in 5 h is not as active as photodegradation according to the UV–vis absorption spectra (Figure 5(a), Figure S5). Reference bead (without vTA-CMp) both at the dark and under visible light show quite similar photodegradation activity with pure RhB solution. Therefore one can strongly conclude that in 5 h, the decreased RhB concentration is solely arising from the photodegradation which is due to vTA-CMp incorporation. As recycling is an essential parameter for photocatalysts, CBT5m was introduced to recycling test owing to its highest photodegradation performance based on previously evaluated RhB photodegradation results. (Figure 5(b), Figure S6). In addition to the depicted dye

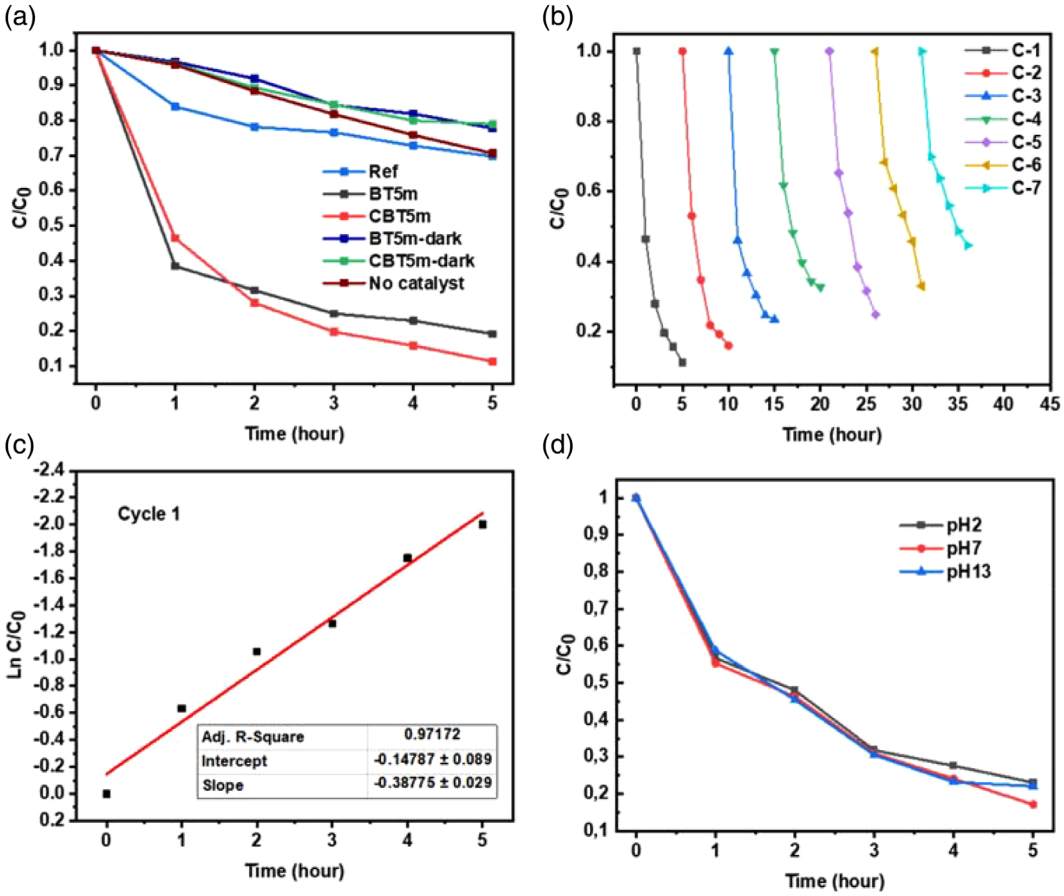

FIGURE 5 (a) RhB dye degradation of BT5M, CBT5m, reference and RhB dye solution (no catalyst) under visible light irradiation (BT5m-dark and CBT5m-dark were not exposed to visible light). (b) Cyclic photocatalytic RhB dye degradation with several run cycles in the presence of CBT5m under visible light irradiation. (c) Pseudo-first order kinetic fitting data of cycle 1 (pH:6.3, T = 25°C, bead/RhB:0.055/0.0015 g.L^{-1} (d) pH effect on photodegradation of CBT5m under visible light irradiation [Color figure can be viewed at wileyonlinelibrary.com]

degradation procedure, employed beads were left in distilled water overnight for the next runafter each completed cycle. As shown in Figure 5(b), degradation efficiencies exhibited slight retardation starting from 89% to 76.5% until the 4th cycle followed by a significant decrease resulting in 55.6% at 7th cycle. Observed downtrend is quite reasonable if surface-attached non-degraded RhB dye molecules are taken into consideration since they are occupying the pores and quantitatively increasing within every run cycle meanwhile not being ultimately released during desorption period. This situation was also observed in adsorption/desorption rate experiment, which will be discussed later on in the following section. Corresponding to the best photoactive performance in which obtained via CBT5m beads, its photodegradation rate constant for RhB dye degradation was examined accordingly. (Figure 5(c)). Regarding the kinetic experiment of the first cycle, samples were collected every 1 h and RhB concentration was monitored by UV–vis spectrum. The adsorption kinetics of CBT5m were fitted to pseudo-first-order rate based on the Langmuir-Hinshelwood model considering reported studies of parental carbon nitride in literature. Regarding that, collected results were calculated according to the integral equation shown here:

$$\ln(Qe - Qt) = \ln Qe - k_1 t$$

Qe is the quantity of dye adsorbed at equilibrium (mg.g^{-1}), Qt is equilibrium concentration at various times t (mg.L^{-1}), and k_1 is the rate constant of adsorption (min^{-1}). As shown in Figure 5(c), the rate constant was determined by the plot of ln (Qe-Qt) versus time. According to pseudo-first-order principle, adsorption rate is proportional to the difference between saturated concentration and adsorption amount of adsorbent thus adsorption is under the control of proceeding diffusion steps. Resulting R^2 value (0.971) of CBT5m beads is quite reasonable yet efficient when free radical polymerization nature in terms of controllability and adjustability to

batch to batch in lab-scale fabrication was considered. On the other hand, the investigation on the photodegradation activity of the pristine vTA-CMp (10 mg/0.01 L) in RhB (4 mg.L^{-1}) solution resulted in 97% degradation in 150 minutes (Figure S7). Reaction rate constant k of RhB photodegradation is 0.0226 min^{-1} for pristine vTA-CMp and 0.0063 min^{-1} (0.38 h^{-1}) for CBT5m bead. One cannot compare the photoactivity of pristine g-CNs with the presented vTA-CMp incorporated polymer network, however the synthesized beads are performing well in comparison to g-CN embedded polymer networks. It should be noted that integration of vTA-CMp in a polymeric network directly influences the primal photodegradation rate constant for RhB. Despite the limitation of vTA-CMp/1-octanol dispersion at higher concentration which undermines the final integration, CBT5M beads (55 mg/0.015 L) resulted in 89% efficiency in 5 h with 3 times recyclability regardless of significant activity loss for RhB photodegredation.

In order to evaluate the pH effect on the photodegradation performance of photoactive beads, CBT5m beads were subjected to RhB solutions in acidic, neutral and alkaline conditions. (Figure 5(d)). As shown in Figure S8, overall photodegradation efficiencies are 82.8%, 77%, 77.8% at pH 2, pH 7, and pH 13, respectively. Generation of photoactive species to perform dye degradation were not influenced by the pH of the media significantly. It is also worth mentioning that CBT5m beads showed very decent physical as well as chemical stability towards strong acidic (pH 2) and basic conditions (pH 13), so that no host degradation products were observed.

3.3 | Dye adsorption and desorption

In addition to photodegradation, the removal of dyes from aqueous systems can be achieved by an adsorption via utilizing an adsorbent by heterogeneous means. Our target in this section is to investigate the synthesized beads for adsorption–desorption performance that relies on physical interactions. For this purpose, model beads were employed into both water-soluble (RhB dye solution) and organo-soluble (Sudan Red 7B and Perylene dye solution, 200 ppm in toluene) dye containing solutions. Regarding RhB aqueous dye solution, model beads were immersed for 24 h for adsorption, then the desorption in clean water was monitored for another 24 h. During the experiment, dye adsorption results were followed via UV–vis spectroscopy (Figure S9). Additionally, reference bead was also included in RhB dye adsorption experiment as a comparison. Referring the absorption spectra results of model and reference beads (Figure S9b), strong adsorption on vTA-CMp containing PS-co-DVB beads compared to a reference was noted. Despite organic character of the beads that prevents water uptake, charged vTA-CMp particles on PS-co-DVB surface can interact with the oppositely charged RhB in solution thus leading to a strong adsorption. Furthermore, dye adsorpt beads were immersed in water for 24 h to investigate the dye desorption (Figure S9d). As expected, model beads released higher dye concentration than reference beads as they have already adsorpt significantly higher amount of dye at the adsorption process. It is worth to mention that this effect is monitored over 24 h and does not have a significant effect during photocalaysis experiments which are conducted for 5 h. Negatively charged vTA-CMP particles render PS-co-DVB beads with a negative charge as well, which is highly promising to be employed as ion exchange resins without further modifications.

In addition, model beads were subjected to adsorption/desorption cycle to evaluate their reusability by first immersing in RhB dye solution then after in distilled water for 24 h for seven times (Figure 6(a)). Until the third run cycle, both adsorption and desorption rates have been quite efficient and satisfactory, but the last 2 cycles exhibited significant desorption activity loss. The reason for the weakened desorption rate over time can be caused by strong electrostatic and hydrophobic interactions between bead surface and dye molecules based on largely diffused dye molecules in each absorption cycle. Besides, limited water access throughout the bead surface based on strong organic nature of PS-DVB beads, which was supported in previous section by water-uptake results, is not providing a favorable condition to similar dye desorption performance thus affecting the next absorption cycle performance. Moreover, pH effect on adsorption/desorption rates of RhB dye were performed by employing model beads at various pH values (Figure 6(b), Figure S10). The most efficient dye uptake performances were obtained both in neutral media (with 63% efficiency) and in basic media (performing 60% efficiency). Adsorption in acidic media has decreased significantly, thus the potential of the beads as adsorption materials should be monitored from neutral to basic media. The most importantly, physical and chemical stability of the beads were confirmed over wide pH range, which offers a potential for chromatographic applications.

Meanwhile, for organosoluble dye system, model beads were employed in two different dye solutions prepared in toluene, and a very fast dye adsorption was visually observed at frequent time intervals (Figure S11). This quick adsorption property can be remarkably useful in organic pollution treatment in aqueous media. As a

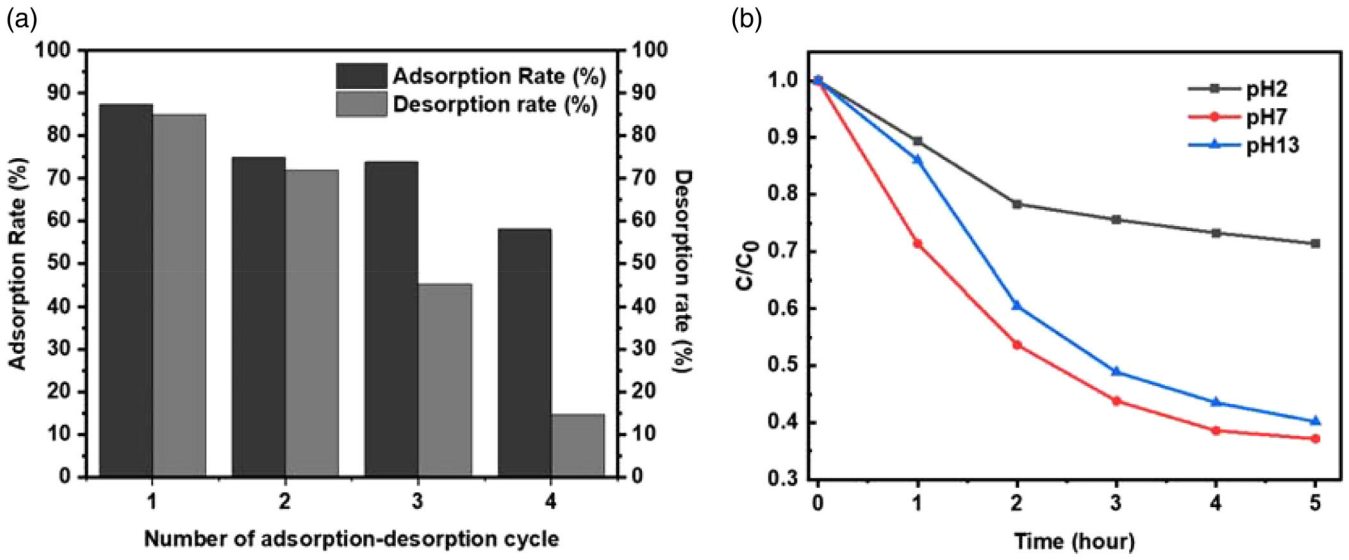

FIGURE 6 (a) Adsorption/desorption rate versus number cycles plot of model bead (24 h time interval). (b) pH effect on adsorption rate of model bead [Color figure can be viewed at wileyonlinelibrary.com]

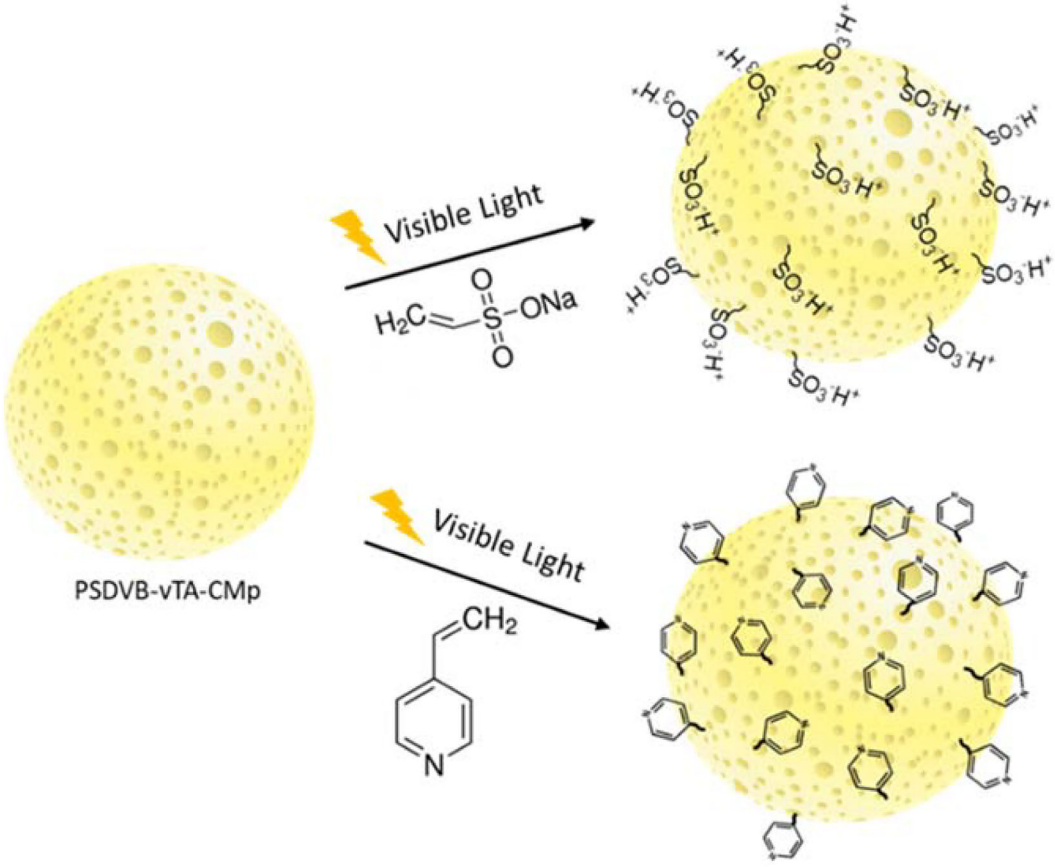

SCHEME 3 Schematic overview of photo-induced surface modification of PS-co-DVB-vTA-CMp beads via visible light irradiation [Color figure can be viewed at wileyonlinelibrary.com]

simulation of recyclability, organic dye immersed beads were placed in toluene and desorption progress was followed (Figure S12). Dye releasing duration was not as fast as adsorption but even after 3 h, toluene had to be replaced to complete a desorption. At the end of the 24 h, a fair amount of adsorbed organic dyes were released

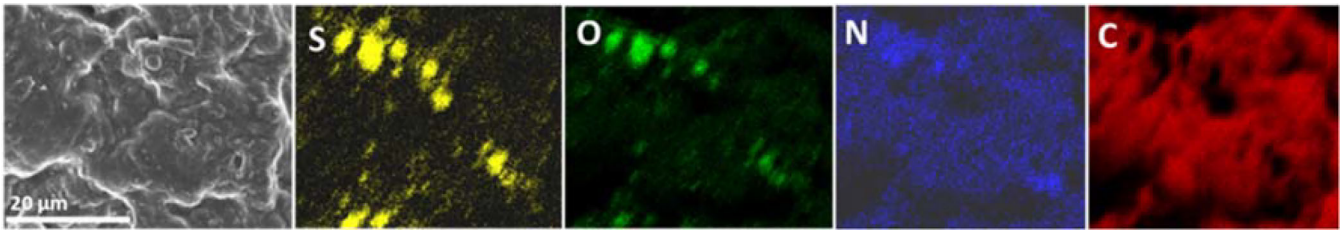

FIGURE 7 Elemental mapping results of CBT5m-VSA via EDX [Color figure can be viewed at wileyonlinelibrary.com]

from the beads. This simple but considerably useful dye adsorption/desorption experiment indicates that vTA-CMp incorporated PS-co-DVB beads have a high capacity toward two different dyes, even though organosoluble dye concentration in this experiment was set to be much higher than a regular pollution concentrations in an environment.

TABLE 2 Combustive elemental analysis results before and after surface modification of CBT5m via VSA and VP

Name	N (%)	C (%)	H (%)	S (%)	C/N
CBT5m	0.96	82.22	8.14	0.08	85.51
CBT5m-VSA	1.05	80.91	8.72	1,44	77.06
CBT5m-VP	1.08	89.52	8.17	0.3	82.91

3.4 | Surface modification of PS-co-DVB-vTA-CMp beads via visible light irradiation

Surface modification of inactive PS-co-DVB resin beads is enabled via introduction of photoactive species, such as vTA-CMp in this case. It is important to reside surface functional groups at the accessible sites, and as vTA-CMp has dispersibility in 1-octanol and no dispersibility in toluene phase, they are ideally located at the interface. To perform post-modification, CBT5m beads were chosen as a model sample due to the highest photoactivity according to the RhB dye degradation results, and vinylic compounds such as vinysulfonic acid (VSA) and 4-vinylpyridine (VP) were employed as reactive monomers (Scheme 3).

As depicted in the preparation section, CBT5m beads were separately immersed in VSA monomer solution prepared with water:DMF mixture and in pure VP. DMF was added in addition to water for VSA modification because of inherent organic character of CBT5m beads, which might obstruct water-soluble monomer accessibility throughout the pores. Immersed beads were placed in front of a visible light and left for overnight (~12 h) under medium agitation to complete the modification. After the purification step, VSA and VP functionalizations were investigated by elemental mapping via EDX, combustive elemental analysis and FTIR.

Regarding VSA grafting, CBT5m-VSA is exhibiting sulfur and oxygen signals, which align with the nitrogen atoms as expected, since nitrogen signifies catalytically active sites where VSA monomers are grafted on the surface (Figure 7).

Furthermore, sulfur content was supported also via combustive elemental analysis up to 1.44 wt% (Table 2). However, VSA modification was not detected via FTIR analysis even though increased reaction time and DMF ratio. This might be explained with low monomer grafting or short propagation.

On the other hand, VP functionalization can be confirmed via combustive elemental analysis based upon increased nitrogen and carbon content (Table 2) along with FTIR spectrum result which displays introduced C═C aromatic stretching vibration at 1597 cm^{-1} and C═N double bond stretching at 1416 cm^{-1} (Figure S13). In addition, CBT5m-VP shows altered luminescence under UV light irradiation (Figure S14).

Preliminary results on visible light induced surface modification are highly intriguing, however in near future extending the vTA-CMp amount in the beads thus improving the amount of photoinduced functionalities and their corresponding catalytic performances will be investigated.

4 | CONCLUSION

In this contribution, organodispersible vTA-CMp containing PS-co-DVB beads were successfully synthesized via UV light induced suspension polymerization. The effects of cross-linker ratio, solvent presence, and agitation were examined in detail. Tunability of the recipe has been demonstrated, and the incorporation of vTA-CMp into polymer network was confirmed by methods such as electron microscopy, UV–Vis and PL. A possibility to employ industrial recipe, thermal initiation, was exhibited briefly. As a model application of the beads, aqueous RhB dye photodegradation experiments were performed. In order to compare a photodegradation activity with the possible physical dye adsorption, same

experiments were also simultaneously performed without visible light irradiation and results clearly showed that rather than dye adsorption, photocatalytic dye degradation occurs. Enhanced photoactivity of the beads was noted when vTA-CMp is utilized as a photoactive component. Organophilicity of the so-formed beads was confirmed via organosoluble dye (Sudan red 7B, perylene) adsorption from a biphasic systems. Adsorption–desorption of aqueous and organic dyes were monitored in addition. A first try on the visible light induced surface modification of PS-co-DVB-vTA-CMp beads was demonstrated, and such approach promises benign surface modifications to be applied from lab to industrial scale.

Bringing g-CN into organic media, which has been quite a challenge until recently, now enables a significant broadening of applications. Herein, we have rendered one of the most commercial polymers, PS-co-DVB beads, with photoactivity via g-CN addition by sticking to the traditional suspension polymerization. In such a way, organodispersible g-CN could be used to decorate the inner pore system, donating photoactivity to such resins, which in turn increases the lifetime and reusability of the photocatalyst by surface heterogenisation and brings it to bead-based reaction columns and automated synthesizers.

ACKNOWLEDGMENT

The authors greatly acknowledge Max Planck Society for funding. Ms. Antje Volkel is acknowledged for TGA measurement, and we appreciate the help from electron microscopy team of MPIKG. Open Access funding enabled and organized by Projekt DEAL.

ORCID

Baris Kumru https://orcid.org/0000-0002-1203-4019

REFERENCES

[1] G. Liao, F. He, Q. Li, L. Zhong, R. Zhao, H. Che, H. Gao, B. Fang, *Prog. Mater. Sci.* **2020**, *112*, 100666.
[2] N. Rono, J. K. Kibet, B. S. Martincigh, V. O. Nyamori, *Crit. Rev. Solid State Mater. Sci.* **2020**, *47*, 1.
[3] S. Cao, J. Low, J. Yu, M. Jaroniec, *Adv. Mater.* **2015**, *27*, 2150.
[4] K. Xiao, P. Giusto, L. Wen, L. Jiang, M. Antonietti, *Angew. Chem. Int. Edit.* **2018**, *57*, 10123.
[5] Z. Sun, W. Wang, Q. Chen, Y. Pu, H. He, W. Zhuang, J. He, L. Huang, *J. Mater. Chem. A* **2020**, *8*, 3160.
[6] W. Xiong, F. Huang, R. Q. Zhang, *Sustain. Energ. Fuels* **2020**, *4*, 485.
[7] A. Naseri, M. Samadi, A. Pourjavadi, A. Z. Moshfegh, S. Ramakrishna, *J. Mater. Chem. A* **2017**, *5*, 23406.
[8] W.-J. Ong, L.-L. Tan, Y. H. Ng, S.-T. Yong, S.-P. Chai, *Chem. Rev.* **2016**, *116*, 7159.
[9] J. Liu, H. Wang, Z. P. Chen, H. Moehwald, S. Fiechter, R. van de Krol, L. Wen, L. Jiang, M. Antonietti, *Adv. Mater.* **2015**, *27*, 712.
[10] Y. Xia, D. K. Xiao, B. Cheng, J. Yu, L. Jiang, M. Antonietti, S. Cao, *ChemSusChem* **2020**, *13*, 1730.
[11] Z. Zhao, Y. Sun, F. Dong, *Nanoscale* **2015**, *7*, 15.
[12] B. Kumru, M. Antonietti, *Adv. Colloid Interface Sci.* **2020**, *283*, 102229.
[13] M. Majdoub, Z. Anfar, A. Amedlous, *ACS Nano* **2020**, *14*, 12390.
[14] H. Yang, Z. Wang, S. Liu, Y. Shen, Y. Zhang, *Chin. Chem. Lett.* **2020**, *31*, 3047.
[15] D. Han, D. Ni, Q. Zhou, J. Ji, Y. Lv, Y. Shen, S. Liu, Y. Zhang, *Adv. Funct. Mater.* **2019**, *29*, 1905576.
[16] Q. Fu, Q. Ruan, T. G. McKenzie, A. Reyhani, J. Tang, G. G. Qiao, *Macromolecules* **2017**, *50*, 7509.
[17] L. Zhang, G. Ye, X. Huo, S. Xu, J. Chen, K. Matyjaszewski, *ACS Omega* **2019**, *4*, 16247.
[18] B. Kumru, D. Cruz, T. Heil, M. Antonietti, *Chem. Mater.* **2020**, *32*, 9435.
[19] B. Kumru, V. Molinari, M. Hilgart, F. Rummel, M. Schaeffler, B. V. K. J. Schmidt, *Polym. Chem.* **2019**, *10*, 3647.
[20] Q. Cao, T. Heil, B. Kumru, M. Antonietti, B. V. K. J. Schmidt, *Polym. Chem.* **2019**, *10*, 5315.
[21] Q. Cao, J. Barrio, M. Antonietti, B. Kumru, M. Shalom, B. V. K. J. Schmidt, *ACS Appl. Polym. Mater.* **2020**, *2*, 3346.
[22] Y. Zhang, Z. Zhou, Y. Shen, Q. Zhou, J. Wang, A. Liu, S. Liu, Y. Zhang, *ACS Nano* **2016**, *10*, 9036.
[23] B. Kumru, D. Cruz, T. Heil, B. V. K. J. Schmidt, M. Antonietti, *J. Am. Chem. Soc.* **2018**, *140*, 17532.
[24] N. Yandrapalli, T. Robinson, M. Antonietti, B. Kumru, *Small* **2020**, *16*, 2001180.
[25] D. Cruz, J. G. Cerrillo, B. Kumru, N. Li, J. D. Perea, B. V. K. J. Schmidt, I. Lauermann, C. J. Brabec, M. Antonietti, *J. Am. Chem. Soc.* **2019**, *141*, 12322.
[26] V. Chaudhary, S. Sharma, *J. Polym. Res.* **2019**, *26*, 102.
[27] M. Grochowicz, B. Gawdzik, *J. Porous Mater.* **2013**, *20*, 339.
[28] C. A. McNamara, M. J. Dixon, M. Bradley, *Chem. Rev.* **2002**, *102*, 3275.
[29] Production of synthetic polymeric compositions comprising aminated polymerizates of poly-vinyl aryl compounds and treatment of liquid media therewith, Google Patents, **1944**.
[30] M. A. Harmer, Q. Sun, *Appl. Catal. A* **2001**, *221*, 45.
[31] P. Gupta, S. Paul, *Catal. Today* **2014**, *236*, 153.
[32] B. Wang, W. Ran, *Chem. Eng. Commun.* **2012**, *199*, 1236.
[33] D. C. Sherrington, *Chem. Commun.* **1998**, *1998*, 2275.
[34] M. P. Tsyurupa, V. A. Davankov, *React. Funct. Polym.* **2006**, *66*, 768.
[35] M. Albuszis, P. J. Roth, W. Pauer, H.-U. Moritz, *Polym. Chem.* **2014**, *5*, 5689.
[36] M. Lavén, T. Alsberg, Y. Yu, M. Adolfsson-Erici, H. Sun, *J. Chromatogr. A* **2009**, *1216*, 49.
[37] S. Weigel, R. Kallenborn, H. Hühnerfuss, *J. Chromatogr. A* **2004**, *1023*, 183.
[38] M. Moeder, S. Schrader, M. Winkler, P. Popp, *J. Chromatogr. A* **2000**, *873*, 95.
[39] J. D. Cahill, E. T. Furlong, M. R. Burkhardt, D. Kolpin, L. G. Anderson, *J. Chromatogr. A* **2004**, *1041*, 171.
[40] M. W. F. Nielen, R. W. Frei, U. A. T. Brinkman, *J. Chromatogr. Libr.* **1988**, *39*, 5.
[41] M. M. Hassan, C. M. Carr, *Chemosphere* **2018**, *209*, 201.
[42] K. Hong, X. Ni, Z. Shen, *Rubber Chem. Technol.* **2016**, *89*, 700.

[43] J. Lu, P. H. Toy, *Chem. Rev.* **2009**, *109*, 815.
[44] M. Benaglia, A. Puglisi, F. Cozzi, *Chem. Rev.* **2003**, *103*, 3401.
[45] H. P. Hentze, M. Antonietti, *Rev. Mol. Biotechnol.* **2002**, *90*, 27.
[46] B. Karagoz, G. Bayramoglu, B. Altintas, N. Bicak, M. Y. Arica, *Ind. Eng. Chem. Res.* **2010**, *49*, 9655.
[47] Q. Li, S. Jin, B. Tan, *Sci. Rep.* **2016**, *6*, 31359.
[48] D. F. Liu, Y. J. Xiang, X. C. Wu, Z. X. Zhang, L. F. Liu, L. Song, X. W. Zhao, S. D. Luo, W. J. Ma, J. Shen, W. Y. Zhou, G. Wang, C. Y. Wang, S. S. Xie, *Nano Lett.* **2006**, *6*, 2375.
[49] P. Cyganowski, A. Dzimitrowicz, *Polymer* **2020**, *12*, 784.
[50] P. A. G. Cormack, A. Davies, N. Fontanals, *React. Funct. Polym.* **2012**, *72*, 939.
[51] O. Ozer, A. Ince, B. Karagoz, N. Bicak, *Desalination* **2013**, *309*, 141.
[52] P. Veverka, K. Jeřábek, *React. Funct. Polym.* **1999**, *41*, 21.
[53] A. Unciti-Broceta, E. M. V. Johansson, R. M. Yusop, R. M. Sánchez-Martín, M. Bradley, *Nat. Protoc.* **2012**, *7*, 1207.
[54] W. Bauman, J. Eichhorn, *J. Am. Chem. Soc.* **1947**, *69*, 2830.
[55] C. W. Huck, G. K. Bonn, *Chem. Eng. Technol.* **2005**, *28*, 1457.
[56] S. Moulay, *Polym. Plast. Technol. Eng.* **2018**, *57*, 1045.
[57] B. Kumru, B. Gure, N. Bicak, *J. Polym. Sci., Part A: Polym. Chem.* **2013**, *51*, 3892.
[58] C. Chen, N. Janoszka, C. K. Wong, C. Gramse, R. Weberskirch, A. H. Gröschel, *Angew. Chem., Int. Ed.* **2021**, *60*, 237.
[59] Q. Cui, J. Xu, X. Wang, L. Li, M. Antonietti, M. Shalom, *Angew. Chem., Int. Ed.* **2016**, *55*, 3672.
[60] P. Giusto, B. Kumru, J. Zhang, R. Rothe, M. Antonietti, *Chem. Mater.* **2020**, *32*, 7284.
[61] M. Yin, Z. Li, J. Kou, Z. Zou, *Environ. Sci. Technol.* **2009**, *43*, 8361.
[62] Y. Jiang, Z. Jin, C. Chen, W. Duan, B. Liu, X. Chen, F. Yang, J. Guo, *RSC Adv.* **2017**, *7*, 12856.
[63] D. Tu, H. Liao, Q. Deng, X. Liu, R. Shang, X. Zhang, *RSC Adv.* **2018**, *8*, 21905.
[64] Q. Cao, B. Kumru, M. Antonietti, B. V. K. J. Schmidt, *Mater. Horiz.* **2020**, *7*, 762.

SUPPORTING INFORMATION

Additional supporting information may be found online in the Supporting Information section at the end of this article.

How to cite this article: Esen C, Antonietti M, Kumru B. Upgrading poly(styrene-co-divinylbenzene) beads: Incorporation of organomodified metal-free semiconductor graphitic carbon nitride through suspension photopolymerization to generate photoactive resins. *J Appl Polym Sci*. 2021;138:e50879. https://doi.org/10.1002/app.50879